Letters in Applied NanoBioScience
Open-Access Journal (ISSN: 2284-6808)

Article
Volume 13, Issue 1, 2024, 27
https://doi.org/10.33263/LIANBS131.027

Effect of Concentration of Acetic Acid Solution on Properties of SF/CS Composite Polymer Scaffold

Pei-Ru Chen [1], Yun-Ju Chuang [1,*]

[1] Department of Biomedical Engineering, Ming Chuan University, Taiwan, R.O.C
* Correspondence: yjchuang@mail.mcu.edu.tw (Y.-J.C.);

Scopus Author ID 7202686959
Received: 4.12.2022; Accepted: 9.01.2023; Published: 13.08.2023

Abstract: Tissue engineering requires nontoxic and biocompatible artificial scaffolds to recover the normal functions of damaged tissues and organs. This study successfully prepared the silk fibroin/chitosan (SF/CS) composite scaffolds by blending silk fibroin and chitosan with different acetic acid concentrations via freeze-drying and glutaraldehyde crosslinking methods. The FTIR spectra confirmed the SF/CS scaffold's internal structural changes from silk fibroin and chitosan to more stable conformation. The degradation rate was steady for up to 60 days. The hematoxylin and eosin (H&E) stained results showed that the internal structure of the SF/CS composite scaffold was porous and three-dimensional, and the SF/CS scaffold with 1 wt% acetic acid solution had relatively uniform pore distribution. The MTT and LDH assay showed that the 1 wt% scaffold group could promote the proliferation of PC-12 cells and lower cell cytotoxicity significantly compared with the control and 1.25 wt% group. Thus, SF/CS with 1 wt% acetic acid solution is a good candidate scaffold for nerve tissue engineering.

Keywords: scaffold; silk fibroin; chitosan; PC-12 cell.

1. Introduction

In the past few decades, scientists and researchers have been trying to recover the normal function of human tissues from injuries based on the rapid and emerging development of functional biomaterials and tissue engineering [1,2]. For nerve injury, the current common way of treatment is a surgical operation, i.e., through suturing the epineural, veins, and muscles. In the case of a small injury gap of the nerve, epineural sutures might be an effective way for nerve function recovery. But for the case of a large injury gap of nerve, challenges will be met by the method of epineural sutures, and the efficacy of nerve function recovery is still insufficient [3]. In addition to the way of surgical operation, some alternative ways can be chosen to recover the function of the nerve, including decellularized injectable peripheral nerve (iPN) matrix [4], acellular nerve allografts (ANA), nerve guidance conduits [5,6], pharmacotherapy [7] and cell therapy [8]. These methods have their disadvantages and limitations under applications. The peripheral nerve (iPN) matrix has biocompatibility issues [9], acellular nerve allografts have to overcome undesirable immunological rejection [10], and cell therapies may have the concern regarding tumorigenicity mainly from the undifferentiated or transformed cells [11].

The ECM is a complex three-dimensional network composed of biomolecules, such as collagen, enzymes, glycoproteins, and hydroxyapatite, that crosslink to provide stable structure

support to surrounding cells. The ECM also regulates the fundamental functions of cells, such as proliferation, adhesion, migration, and differentiation [12,13]. The well-designed artificial scaffolds can be utilized as a biomimicking ECM to provide proper properties such as biocompatibility, electrical conductivity, and hydrophilicity necessity for cell adhesion, cell-to-cell communication, and differentiation [14].

Polymer, metal, and ceramics are the common materials used for scaffold fabrication to provide a suitable template for cell and tissue regeneration. The selection of materials to prepare scaffolds for tissue engineering has concerns regarding biocompatibility, wettability, mechanical strength, and biodegradability [15]. Polymers, including natural and synthetic polymers, have been used to prepare tissue engineering scaffolds to enhance the repair processes of damaged tissues [16,17]. Synthetic polymers have excellent mechanical strength and adjustable biodegradability characteristics, but poor biocompatibility limits further applications [18].

Natural polymers have been widely used to develop scaffolds due to their enhanced immunogenic and biocompatibility properties [19]. The common natural polymers used in preparing tissue-engineered scaffolds are chitosan, collagen, gelatin, silk fibroin, alginate, etc [20]. Among these natural polymer materials, chitosan and silk fibroin have drawn much attention as candidate biomaterials suitable for fabricating scaffolds. Silk fibroin, a nontoxic biomaterial obtained from silkworm cocoon, has been used in many biomedical applications, benefiting from excellent mechanical strength, permeability and biocompatibility, controllable biodegradability, and shaping adaptability [21-23]. Chitosan is another widely used biomaterial made by deacetylation of chitin obtained from shells of crustaceans and also is biocompatible and biodegradable. More importantly, the chemical structure of chitosan is similar to an extracellular matrix (ECM), and the surface is hydrophilic. Both characteristics significantly promote the adhesion, proliferation, and differentiation of cells for the repair of injured tissues [24,25]. The use of CS and SF alone as a scaffold has demonstrated the ability to promote cell proliferation for tissue engineering applications [26, 27]. Combining CS and SF to form SF/CS composite film or three-dimensional scaffolds exhibits both SF and CS advantages, such as ECM mimic nature, non-toxicity, biodegradability, anti-inflammatory, hydrophilic surface, and antibacterial properties [28]. The properties of SF/CS composites can be adjusted by tuning the mixing ratio of silk fibroin and chitosan. Furthermore, neutralizing negative charge SF and positive charge chitosan in SF/CS composites can offer better hemocompatibility than using CS alone.

This study blended silk fibroin and chitosan with different acetic acid concentrations to create a three-dimensional scaffold with controllable pore size and mechanical properties. The morphology, mechanical strength, degradation rate, and PC12 nerve cell culture viability of the SF/CS composite scaffolds were investigated.

2. Materials and Methods

2.1. Preparation of SF solution.

The natural silk was washed in 40 °C warm water to remove impurities and dried in the oven at 50 °C. 2 g of raw silk was added into 300 mL of 0.5 % (w/v) sodium carbonate solution and placed in a water bath at 100 °C for 1 h to degumming. The degummed silk was drained from the sodium carbonate solution and rinsed with deionized water 20 times. Then, the

degummed silk was carefully washed with deionized water to remove any remaining sericin coating on the silk and air-dried.

The degummed silk was dissolved in a calcium dichloride and ethanol mixed solution with molar ratio $CaCl_2 : H_2O : C_2H_5OH = 1 : 8 : 2.5$ at 80 °C and stirred continuously for 1 h. After cooling down, the silk solution was dialyzed against deionized water to remove calcium dichloride and ethanol. Finally, the silk fibroin solution was adjusted to the desired concentration and stored at 4 °C until use.

2.2. Fabrication of silk fibroin/chitosan (SF/CS) scaffold.

Chitosan solutions were prepared by completely dissolving chitosan powder in 1 and 1.25 wt% acetic acid solution. SF and CS were mixed in a volume ratio of 3 : 1 to prepare a 3 and 1 wt% blended solution and the solution was mixed for 15 min at room temperature, followed by adding 3 mL 0.5 wt% glutaraldehyde for cross-linkage. The SF/CS blended solution was poured into a circular PTFE mold with a diameter of 10 mm, and stored at -20 °C for 30 min and then at -80 °C overnight. The dry SF/CS sample was obtained by lyophilization for 24 h. Then, the SF/CS sample was treated in methanol for 1 h and followed by rinsing in PBS. Finally, the SF/CS scaffold was completely prepared by another lyophilization for 24 h.

2.3. Characterization.

The mechanical compression resistance properties of the SF/CS scaffold were performed on a ZTA-5N force tester equipped with a 0.1 kN load cell at room temperature. The scaffold sample was prepared as a cylinder of 10 mm in diameter and 10 mm in height. The tensile stress and strain were recorded, and the elastic modulus of the scaffold was determined from the stress-strain curve by using the following equation: $E=FL/S\Delta L$, where L and S are the length and cross-sectional area of the scaffold, and ΔL is the extended length of the scaffold corresponding to the applied force F.

For the characterization of SF, CS, and SF/CS, FTIR spectroscopy (FT/IR 6000, JASCO) was used to identify structural, conformational, and functional properties. The freeze-dried SF, CS, and SF/CS samples were pressed into pellets with potassium bromide (KBr), and the FTIR spectrum was recorded by JASCO IR Spectrometer with a resolution of 4 cm-1 in the range of 400–4000 cm^{-1}.

The degradation property test of the SF/CS scaffold was performed by placing an SF/CS scaffold block in the sterilized simulated body fluid and incubated at 37 °C in a humidified atmosphere for 1, 3, 6, 9, 12, 15, 22, 29, 36 and 56 days. The scaffold samples were weighed before and after immersing in the simulated body fluid, as wb and wa. The degradation rate was calculated using the formula: (wb-wa)/wb×100%.

2.4. Cell studies.

Rat adrenal pheochromocytoma PC12 cells were used as model neuro cells and were cultured in DMEM culture medium containing 10% fetal bovine serum, 200 mM L-glutamine, 3.7 mg/ml sodium bicarbonate and 100 mg/ml penicillin/streptomycin. Then, PC12 cells were incubated at 37 °C and in a humidified atmosphere containing 5 % CO2. The SF/CS scaffold samples were prepared as circular discs for 96-well culture plate wells. The scaffolds were sterilized with 70% alcohol and then rinsed with a sterile PBS buffer solution. Before culturing with cells, scaffolds were immersed in DMEM culture medium for 12 h in the 37 °C incubator.

PC12 cells were cultured onto SF/CS scaffolds for 1, 3, and 7 days with a cell density of 10000 cells per well.

The cell viability of PC12 cells on SF/CS scaffolds was evaluated by a standard MTT (3-(4, 5-dimethylthiazol-2-yl)-2, 5-diphenyltetrazolium bromide) assay, which is a quantitative colorimetric assay for determining the level of cell growth and proliferation. To perform the MTT assay, the culture medium was discarded, and 200 µl MTT stock solution was added into each well and incubated for another 4 h in the dark. Then, 200 µl DMSO solution was added into each well to dissolve formazan crystals into a colored solution. The absorbance of the colored formazan solution was measured by an ELISA microplate spectrometer at 570 nm.

The cytotoxicity of SF/CS scaffold on PC12 cells was assessed by LDH assay, a quantitative colorimetric assay to measure lactate dehydrogenase (LDH), an enzyme released upon cell death and lysis. To perform the LDH assay, the 100 µl culture medium was transferred to a fresh 96-well plate, and 100 µl LDH reagent mixing solution was added into each well and incubated for 30 min in the dark. Then, 50 µl of stop solution was added to each well, and the absorbance of the medium solution was measured by ELISA microplate spectrometer at 490 nm within 1 hour after adding the stop solution.

3. Results and Discussion

The photo image of the SF/CS composite scaffold is shown in Figure 1. By observing the structure of the SF/CS scaffold with the naked eye, it was found that the color of the SF/CS composite scaffold is yellowish white, and its structure seemed to be flexible and spongy inside with a rough surface. By comparing the SF/CS scaffold with 1 and 1.25 wt% acetic acid solution, we found that the structure of the 1 wt% group was relatively loose, but the 1.25 wt% group was denser. The difference in morphology may be due to the different concentrations of acetic acid solution used to prepare CS solution. The CS solution was prepared with a higher concentration of acetic acid solution, and the content of CS in the CS solution will be higher. Thus, the SF/CS scaffold with higher CS content will form a more compact and dense structure during the subsequent crosslinking process.

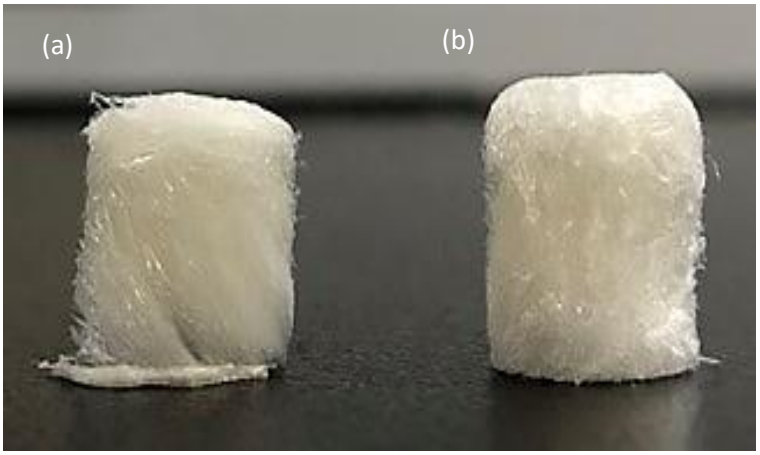

Figure 1. SF/CS scaffold with **(a)** 1 and **(b)** 1.25 wt% acetic acid solution after 24 h lyophilization.

The elastic properties utilizing the tension test of silk fibroin/chitosan scaffold are shown in Figure 2. The elastic modulus of SF/CS scaffold with 1 and 1.25 wt% acetic acid solution was 3.724 ± 0.208 and 6.667 ± 0.373 MPa, and the max strain was 0.06 and 0.04 %, respectively. The elastic property results showed that the 1 wt% group was relatively more

flexible than the 1.25 wt% group, and the results were consistent with the morphology difference shown in Figure 1.

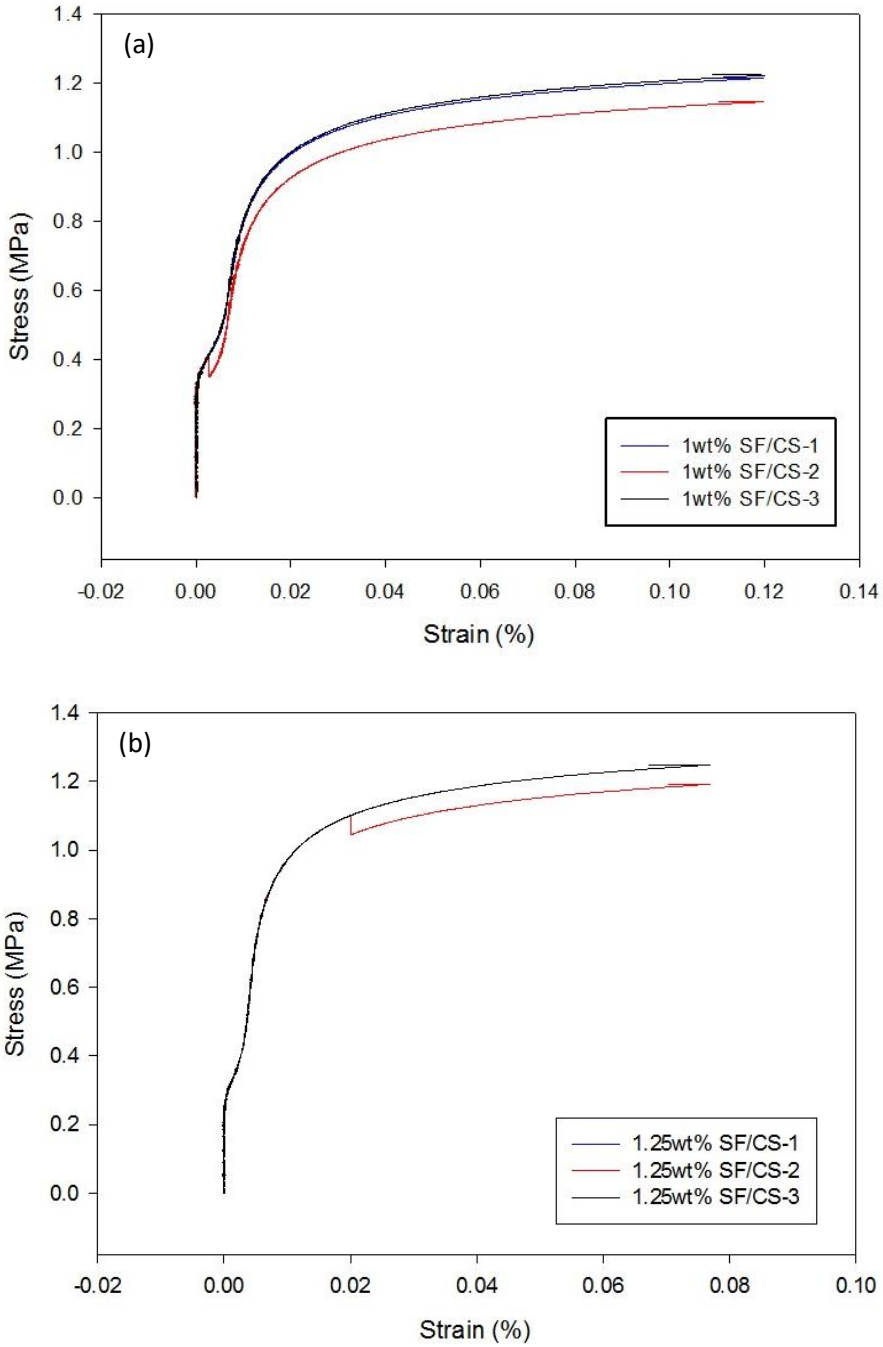

Figure 2. Elastic properties of the silk fibroin/chitosan scaffold with **(a)** 1 and **(b)** 1.25 wt% acetic acid solution.

The infrared analysis results are shown in Figure 3. For pure SF, the absorption peak of amide I, II, and III band were at 1645, 1534, and 1257 cm^{-1}. For pure CS, the characteristic absorption peaks due to the existence of interconnecting β-1,4 glycosidic bonds were found at 1155 and 896 cm^{-1}. The SF/CS scaffold contains SF and CS, and hence the same characteristic absorption peaks of β-1,4 glycosidic bond as CS were observed at 1153 and 899 cm^{-1}, and also the same amide I band peaks as SF were at 1632-1635 cm^{-1}, and the characteristic absorption peaks were reduced when compared with pure SF and pure CS.

The absorption peak of the amide I band at 1645 cm^{-1} indicated that the existence of α-helix structure and the characteristic peak of amide II and III band at 1534 and 1257 cm^{-1} suggested the random coil structure of SF [29]. Therefore, the conformation of pure SF was

mainly dominated by α-helix and random coil structure, leading to unstable and poor mechanical properties. For SF/CS composite scaffold, the absorption peak of the amide I band shifted to 1632-1635 cm^{-1}, representing the β sheet conformation. From the infrared analysis results, it was suggested that the mixing of CS and SF effectively modified and enhanced the structure of SF and made the unstable α-helix and random coil structure transform into relatively stable β sheet conformation.

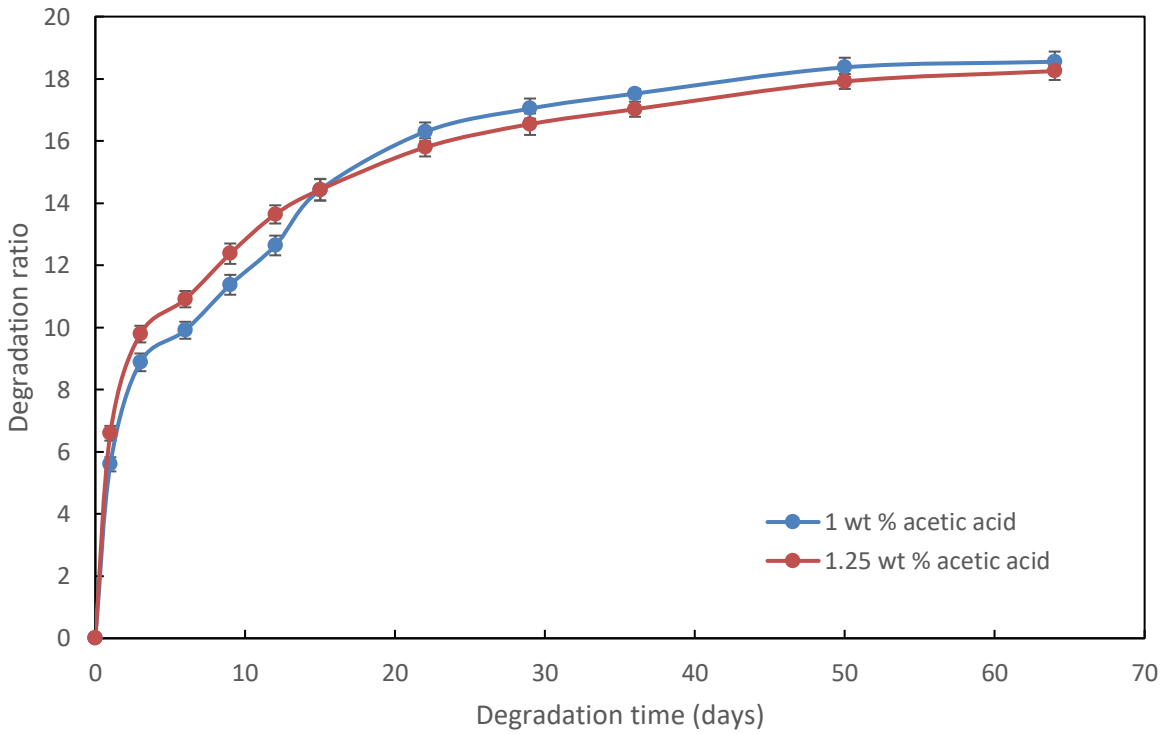

Figure 3. FTIR spectra of SF, CS, and SF/CS scaffold.

The results of the degradation rate of the SF/CS scaffold with 1 and 1.25 wt% acetic acid solution are shown in Figure 4. In the first 3 days, the degradation rate of the SF/CS scaffold was highest for both groups. At 3 to 36 days, the degradation rate slowed down, and about 17% of the original weight had been degraded since the beginning of the experiment. From 36 to 64 days, the degradation rate was further decreased, and by day 64, the SF/CS scaffold had lost about 18% weight since the beginning of the degradation experiment.

The scaffold materials should provide a steady and appropriate degradation rate to match the cells' growth rate during in vitro cell growth [30-32]. That is, the degradation rate of the scaffold should match the growth rate of new tissue. Therefore, when the new tissue is fully formed, the scaffold must be able to degrade completely and be absorbed by the human body. In the present study, the degradation rate of the SF/CS scaffold was stable and thus can be considered as having potential for application in vivo experiments.

The images of hematoxylin and eosin (H&E) stained SF/CS scaffold sections are shown in Figure 4. The purplish-blue part represented the PC12 cells, while the red represented the SF/CS scaffold structures. After 3 days of incubation with PC12 cells, the cells uniformly adhered and grew in the porous SF/CS scaffold structures. By inspecting the internal structure of SF/CS composite material through the hematoxylin and eosin (H&E) stained section, it can be found that a porous structure inside the scaffold with a clear connective network structure exists. The stained sections' images revealed that the SF/CS scaffold morphology with 1 wt%

acetic acid solution was better than 1.25 wt%. It had relatively small and uniformly distributed pores and better connectivity between pores. Therefore, the adhesion and growth of PC12 cells on the 1% SF/CS scaffold were better than that on the 1.25% SF/CS scaffold.

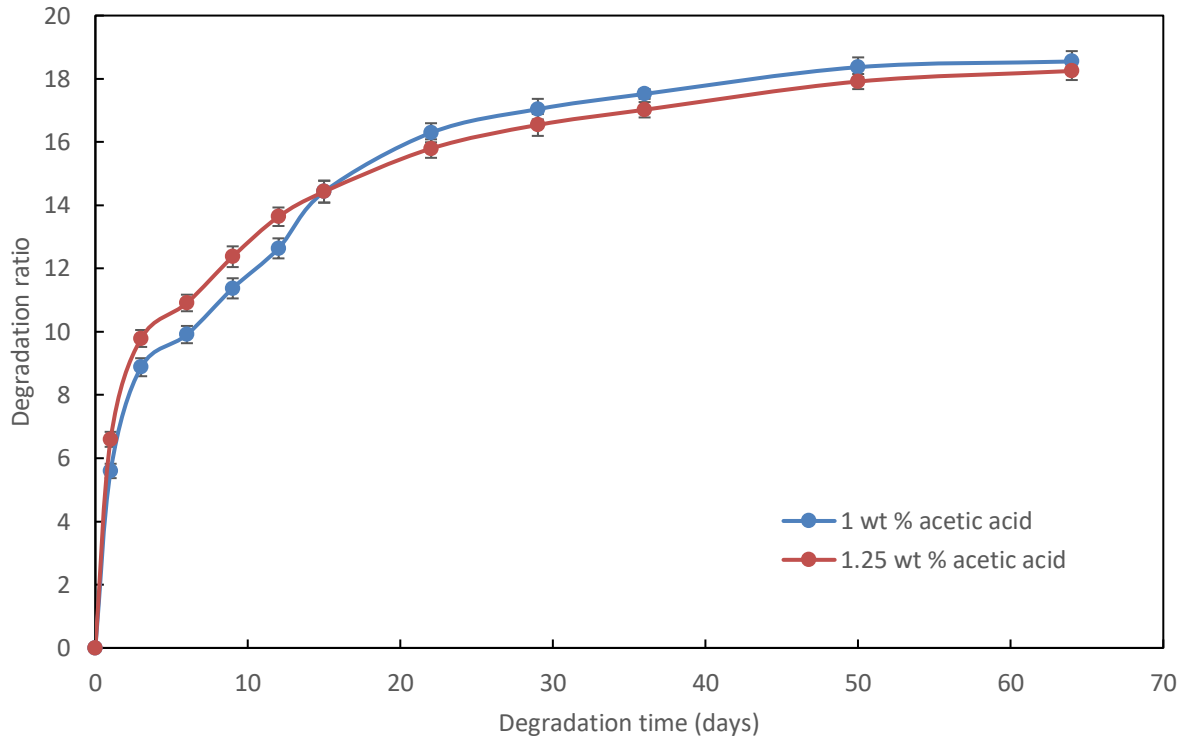

Figure 4. The degradation rate of the silk fibroin/chitosan scaffold with 1 and 1.25 wt% acetic acid solution.

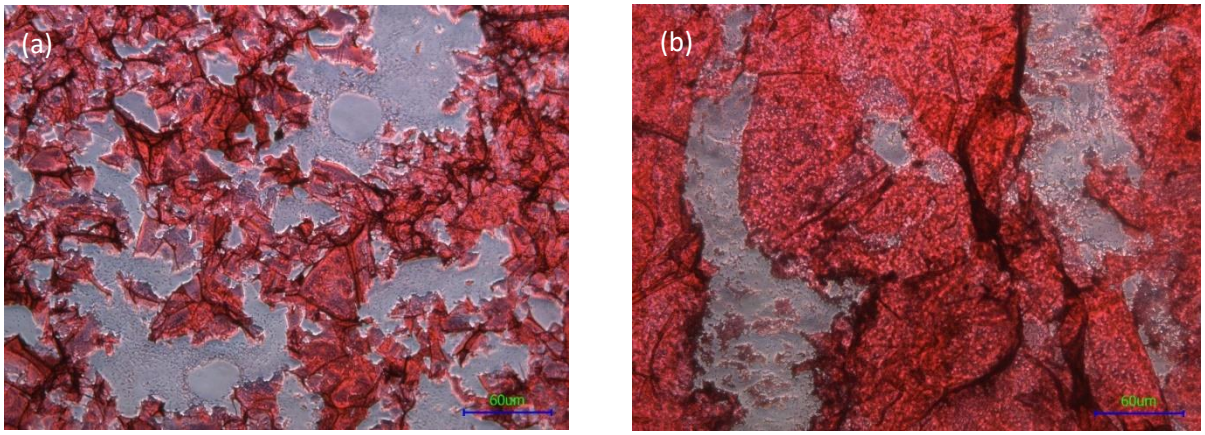

Figure 5. The hematoxylin and eosin (H&E) stained image showing PC12 cells growth on the SF/CS scaffold material with **(a)** 1 wt% and **(b)** 1.25 wt% acetic acid solution.

The results of PC-12 cell proliferation in different scaffold groups and at different culture times are shown in Table 1 and Figure 6. The proliferation rates of 1 wt% and 1.25 wt% groups were significantly higher than the control group at all culture time points. On day one, there were no statistically significant differences in cell proliferation between the two scaffold groups. On days three and seven, the cell proliferation rate in the 1 wt% group was significantly higher than that in the 1.25 wt% group. The PC-12 cell cytotoxicity results revealed by absorption OD values in different scaffold groups and at different culture times are shown in Table 2 and Figure 7. The cytotoxicity of both scaffold groups was significantly lower than the control group at all culture time points. On days one and seven, the cell cytotoxicity in the 1 wt% group was significantly higher than that in the 1.25 wt% group. On day three, there were

no statistically significant differences in cell cytotoxicity between the two scaffold groups. The 1 wt% scaffold group demonstrated a higher PC-12 cell proliferation rate and lower cytotoxicity than the control and 1.25 wt% groups. The enhanced effects could be attributed to the small, uniformly distributed, well-connected porous structures inside the scaffold.

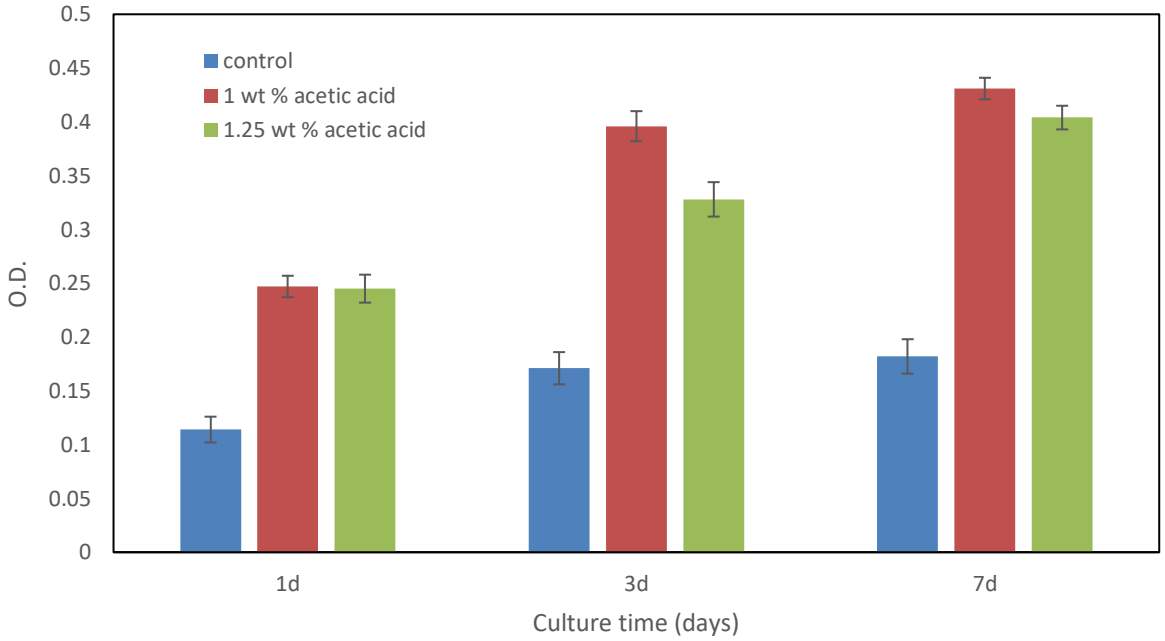

Figure 6. PC-12 cell proliferation in different scaffold groups and at different culture time points.

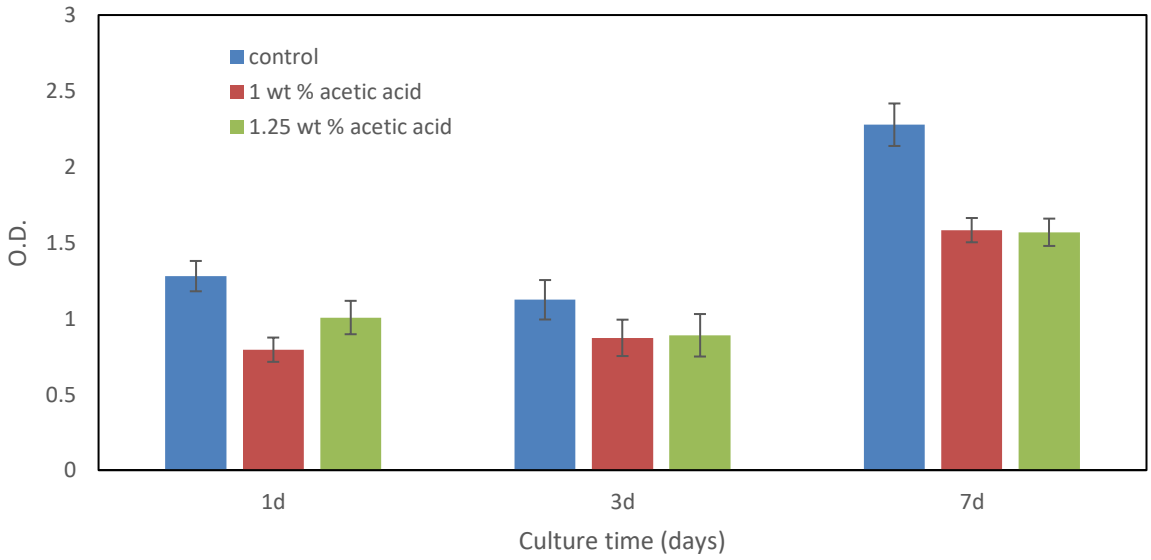

Figure 7. PC-12 cell cytotoxicity in different scaffold groups and at different culture time points.

Table 1. PC-12 cells proliferation rates at different time points ($\bar{x}$±s, n = 5).

Group	**Culture Time**		
	1 d	3d	7d
Control	0.114±0.009	0.171±0.011	0.182±0.013
1 wt%	0.247±0.008 ★	0.396±0.012 ★	0.431±0.008 ★
1.25 wt%	0.245±0.010 ★ ▲	0.328±0.014 ★◆	0.404±0.009 ★◆
P value	<0.001	<0.001	<0.001

★ significantly different from the scaffold in the control group (P<0.001).
▲ not significantly different from the 1 wt% group (P>0.05).
◆ significantly different from the 1 wt% group (P<0.001).

Table 2. PC-12 cells cytotoxicity at different time points ($\bar{x}$±s, n = 5).

Group	Culture Time		
	1 d	3d	7d
Control	1.279+-0.047	1.123+-0.102	2.277+-0.110
1 wt%	0.794+-0.063 ★	0.872+-0.094 ◆	1.582+-0.063 ★
1.25 wt%	1.006+-0.087 ★ ▲	0.889+-0.110 ◆●	1.568+-0.071 ★●
P value	<0.001	<0.05	<0.001

★ significantly different from the scaffold in the control group (P<0.001).
▲ significantly different from the 1 wt% group (P<0.05).
◆ significantly different from the scaffold in the control group (P<0.05).
● not significantly different from the 1 wt% group (P>0.05).

4. Conclusions

Chitosan and silk fibroin are natural polymers with good biocompatible and biodegradable properties. Combining chitosan and silk fibroin to form composites can provide better biological properties than a single material. In this study, the SF/CS composite scaffolds were prepared by blending silk fibroin and chitosan with different acetic acid concentrations and obtained by lyophilization. The FTIR analysis results showed the structural changes of SF/CS composite to more stable conformation. The physical tests and hematoxylin and eosin (H&E) stained results showed that the SF/CS scaffold with 1 wt% acetic acid solution exhibited more flexible and uniformly distributed porous structures. The in vitro degradation experiments were performed, and the degradation rate was stable for both SF/CS scaffolds groups for 64 days. The in vitro PC-12 cell culture results showed a significantly higher proliferation rate and lower cell cytotoxicity for both SF/CS scaffolds groups compared with the blank control group. Therefore, this scaffold has great application potential to be used as a scaffold for nerve regeneration.

Funding

This research was funded by the Ministry of Science and Technology of Taiwan, grant number MOST 110-2221-E-130-013.

Acknowledgments

Declared none.

Conflicts of Interest

The authors declare no conflict of interest.

References

1. Mohabatpour, F.; Chen, X.; Papagerakis, S. Novel trends, challenges and new perspectives for enamel repair and regeneration to treat dental defects. *Biomater. Sci.*, **2022**, *10*, 3062-3087, https://doi.org/10.1039/D2BM00072E.
2. Zhao, Y.; Song, S.; Ren, X.; Zhang, J.; Lin, Q.; Zhao, Y. Supramolecular Adhesive Hydrogels for Tissue Engineering Applications. *Chem. Rev.*, **2022**, *122*, 5604-5640, https://doi.org/10.1021/acs.chemrev.1c00815.
3. Wu, J.; Sahoo, J. K.; Li, Y.; Xu, Q.; Kaplan, D. L. Challenges in delivering therapeutic peptides and proteins: A silk-based solution, *J Control Release*, **2022**, *345*, 176-189, https://doi.org/10.1016/j.jconrel.2022.02.011.
4. Wang, M.; Huang, X.; Zheng, H.; Tang, Y.; Zeng, K.; Shao, L.; Li, L. Nanomaterials applied in wound healing: Mechanisms, limitations and perspectives. *J Control Release*, **2021**, *337*, 236-247, https://doi.org/10.1016/j.jconrel.2021.07.017.

5. Lau, Y.-T.; Kwok, L.-F.; Tam, K.-W.; Chan, Y.-S.; Shum, D.K.-Y.; Shea, G.K.-H. Genipintreated chitosan nanofibers as a novel scaffold for nerve guidance channel design, *Colloids Surf. B: Biointerfaces*, **2018**, *162*, 126–134, https://doi.org/10.1016/j.colsurfb.2017.11.061.
6. Sun, B.; Zhou, Z.; Wu, T.; Chen, W.; Li, D.; Zheng, H.; El-Hamshary, H.; Al-Deyab, S.S.; Mo, X.; Yu, Y. Development of nanofiber sponges-containing nerve guidance conduit for peripheral nerve regeneration in vivo, *ACS Appl. Mater. Interfaces*, **2017**, *9*, 26684–26696, https://doi.org/10.1021/acsami.7b06707.
7. Gennari, C.G.; Cilurzo, F.; Mitro, N.; Caruso, D.; Minghetti, P.; Magnaghi, V. In vitro and in vivo evaluation of silk fibroin functionalized with GABA and allopregnanolone for Schwann cell and neuron survival, *Regen. Med.*, **2018**, *13* , 141–157, https://doi.org/10.2217/rme-2017-0102.
8. Jones, I.; Novikova, L.N.; Novikov, L.N.; Renardy, M.; Ullrich, A.; Wiberg, M.; Carlsson, L.; Kingham, P.J. Regenerative effects of human embryonic stem cellderived neural crest cells for treatment of peripheral nerve injury, *J. Tissue Eng. Regen. Med.*, **2018**, *12*, e2099–e2109, https://doi.org/10.1002/term.2642.
9. Li, H.; Ye, A.Q.; Su, M. Application of stem cells and advanced materials in nerve tissue regeneration. *Stem Cells Int.*, **2018**, *2018*, https://doi.org/10.1155/2018/4243102.
10. Boriani, F.; Fazio, N.; Bolognesi, F.; Pedrini, F.A.; Marchetti, C.; Baldini, N. Noncellular modification of acellular nerve allografts for peripheral nerve reconstruction: a systematic critical review of the animal literature, *World Neurosurg.*, **2018**, *122*, 692–703, https://doi.org/10.1016/j.wneu.2018.10.195.
11. Zhou, Y.; Zhao, J.; Sun, X.; Li, S.; Hou, X.; Yuan, X.; Yuan, X. Rapid gelling chitosan/ polylysine hydrogel with enhanced bulk cohesive and interfacial adhesive force: mimicking features of epineurial matrix for peripheral nerve anastomosis, *Biomacromolecules*, **2016**, *17*, 622–630, https://doi.org/10.1021/acs.biomac.5b01550
12. de Almeida, L. G.N.; Thode, H,; Eslambolchi, Y.; Chopra, .; Young, D.; Gill, S.; Devel, L.; Dufour, A. Matrix Metalloproteinases: From Molecular Mechanisms to Physiology, Pathophysiology, and Pharmacology, *Pharmacol. Rev.*, **2022**, *74*, 714-770, https://doi.org/10.1124/pharmrev.121.000349.
13. Bandzerewicz, A.; Gadomska-Gajadhur, A. Into the tissues: extracellular matrix and its artificial substitutes: cell signalling mechanisms.*Cells* **2022**, *11*, 914, https://doi.org/10.3390/cells11050914.
14. Wang, W.; Caetano, G.; Ambler, W.S.; Blaker, J.J.; Frade, M.A.; Mandal, P.; Diver, C.; B'artolo, P. Enhancing the hydrophilicity and cell attachment of 3D printed PCL/ graphene scaffolds for bone tissue engineering. *Materials* **2016**, *9*, 992, https://doi.org/10.3390/ma9120992.
15. Kalirajan, C.; Dukle, A.; Nathanael, A.J.; Oh, T.-H.; Manivasagam, G. A Critical Review on Polymeric Biomaterials for Biomedical Applications. *Polymers*, **2021**, *13*, 3015, https://doi.org/10.3390/polym13173015.
16. Chahal, S.; Kumar, A.; Hussian, F.S.J. Development of biomimetic electrospun polymeric biomaterials for bone tissue engineering. A review. *J. Biomater. Sci. Polym. Ed.*, **2019**, *30*, 1308–1355, https://doi.org/10.1080/09205063.2019.1630699.
17. Mir, M.; Ali, M.N.; Barakullah, A.; Gulzar, A.; Arshad, M.; Fatima, S.; Asad, M. Synthetic polymeric biomaterials for wound healing: A review. *Prog. Biomater.* **2018**, *7*, 1–21, https://doi.org/10.1007/s40204-018-0083-4.
18. Haghighi, P.; Shamloo, A. Fabrication of a novel 3D scaffold for cartilage tissue repair: In-vitro and in-vivo study. *Mater. Sci. Eng. C* **2021**, *128*, 112285, https://doi.org/10.1016/j.msec.2021.112285.
19. Zhang, X.; Shi, X.; Gautrot, J. E.; Peijs, T. Nanoengineered electrospun fibers and their biomedical applications: a review. *Nanocomposites* **2021**, *7*, 1-34, https://doi.org/10.1080/20550324.2020.1857121.
20. Oryan, A., Sahvieh, S. Effectiveness of chitosan scaffold in skin, bone and cartilage healing. *Int. J. Biol. Macromol.* **2017**, *104*, 1003–1011, https://doi.org/10.1016/j.ijbiomac.2017.06.124.
21. Abdollahiyan, P.; Oroojalian, F.; Hejazi, M.; de la Guardia, M.; Mokhtarzadeh, A. Nanotechnology, and scaffold implantation for the effective repair of injured organs: An overview on hard tissue engineering. *J. Control. Release*, **2021**, *333*, 391-417, https://doi.org/10.1016/j.jconrel.2021.04.003.
22. Chen, J. J.; Cheng, G.; Liu, R.; Zheng, Y.; Huang, M.; Yi, Y.; Shia, X.; Du, Y.; Denga, H. Enhanced physical and biological properties of silk fibroin nanofibers by layer-by-layer deposition of chitosan and rectorite. *J. Colloid Interface Sci.* **2018**, *523*, 208–216, https://doi.org/10.1016/j.jcis.2018.03.093.
23. Chen, X.; Cao, X.; Jiang, H.; Che, X.; Xu, X.; Ma, B.; Zhang, J.; Huang, T. SIKVAV-Modified Chitosan Hydrogel as a Skin Substitutes for Wound Closure in Mice. *Molecules* **2018**, *23*, 2611, https://doi.org/10.3390/molecules23102611.
24. Vukajlovic, D.; Parker, J.; Bretcanu, O.; Novakovic, K. Chitosan based polymer/bioglass composites for tissue engineering applications. *Mater. Sci. Eng. C.* **2018**, *96*, 955–967, https://doi.org/10.1016/j.msec.2018.12.026.

25. Kara, A.; Tamburaci, S.; Tihminlioglu, F.; Havitcioglu, H. Bioactive fish scale incorporated chitosan biocomposite scaffolds for bone tissue engineering, *Int. J. Biol. Macromol.* **2019**, *130*, 266–279, https://doi.org/10.1016/j.ijbiomac.2019.02.067
26. Li, Y.; Liu, Y.; Guo, Q. Silk fibroin hydrogel scaffolds incorporated with chitosan nanoparticles repair articular cartilage defects by regulating TGF-β1 and BMP-2. *Arthritis Res Ther* **2021**, *23*, 50, https://doi.org/10.1186/s13075-020-02382-x.
27. Davachi, S. M.; Haramshahi, S. M. A.; Akhavirad, S. A.; Bahrami, N.; Hassanzadeh, S.; Ezzatpour, S.; Hassanzadeh, N.; Kebria, M. M.; Malekzadeh M.; Khanmohammadi, M.; Bagher, Z. Development of chitosan/hyaluronic acid hydrogel scaffolds via enzymatic reaction for cartilage tissue engineering. *Materials Today Communications* **2022**, *30*, 103230, https://doi.org/10.1016/j.mtcomm.2022.103230.
28. Tu, P.; Pan, Y.; Wu, C.; Yang, G.; Zhou, X.; Sun, J.; Wang, L.; Liu, M.; Wang, Z.; Liang, Z.; Guo, Y.; Ma, Y. Cartilage Repair Using Clematis Triterpenoid Saponin Delivery Microcarrier, Cultured in a Microgravity Bioreactor Prior to Application in Rabbit Model. *ACS Biomater. Sci. Eng.* **2022**, *8*, 753-764, https://doi.org/10.1021/acsbiomaterials.1c01101
29. Elliott, A.; Ambrose, E. J. Structure of synthetic polypeptides. *Nature* **1950**, *165*, 921–922, https://doi.org/10.1073/pnas.37.5.241.
30. Dong, W.; Huang, X.; Sun, Y.; Zhao, S.; Yin, J.; Chen, L. Mechanical characteristics and in vitro degradation kinetics analysis of polylactic glycolic acid/β-tricalcium phosphate (PLGA/β-TCP) biocomposite interference screw. *Polym. Degrad. Stab.* **2021**, *186*, 109421, https://doi.org/10.1016/j.polymdegradstab.2020.109421
31. Aiman, A. R.; Vigneswari, S.; Amran, N. A.; Murugaiyah, V.; Amirul, A. A.; Ramakrishna, S. Advancing Regenerative Medicine Through the Development of Scaffold, Cell Biology, Biomaterials and Strategies of Smart Material. *Regen. Eng. Transl. Med.*, **2022**, *8*, 298–320, https://doi.org/10.1007/s40883-021-00227-w.
32. Ou, Y.; Wu, W.; Zhou, Z. In-Vitro Degradation Behaviors of Composite Scaffolds Based on Poly (Lactide-co-Glycolide-co-ε-Caprolactone), 1, 4-Butanediamine Modified Poly (Lactide-co-Glycolide) and Bioceramics. *J. Macromol. Sci. B.* **2022**, *61*, 776-787, https://doi.org/10.1080/00222348.2022.2101972.